Magnesium Technology 2011
Edited by: Wim H. Sillekens, Sean R. Agnew, Neale R. Neelameggham, and Suveen N. Mathaudhu
TMS (The Minerals, Metals & Materials Society), 2011

COMPRESSIVE CREEP BEHAVIOUR OF EXTRUDED Mg ALLOYS AT 150 °C

M. Fletcher[1], L. Bichler[1], D. Sediako[2] and R. Klassen[3]
[1]University of British Columbia – Okanagan, School of Engineering, Kelowna, Canada
[2]Canadian Neutron Beam Centre, Chalk River, Canada
[3]University of Western Ontario, London, Canada

Keywords: Creep, Magnesium Alloys, Nano-Indentation

Abstract

Wrought magnesium alloy bars, sections and tubes have been extensively used in the aerospace, electronics and automotive industries, where component weight is of concern. The operating temperature of these components is typically limited to below 100°C, since appreciable creep relaxation of the wrought alloys takes place above this temperature.

The objective of this study was to investigate the high temperature creep performance of two wrought magnesium alloys (AE42 and EZ33) developed for elevated temperature applications. Compressive creep behavior of extruded rods was studied at room temperature and at 150°C using the nano-indentation creep technique (on the microscale) and neutron diffraction (on the macroscale). Measurements were performed in the extrusion and radial directions to observe the effect of texture on the creep resistance, hardness and elastic modulus of the alloys. Microscopic examination of the alloys revealed that the distribution of second phases along the grain boundaries was critical to the alloy's creep resistance.

Introduction

Magnesium (Mg) is one of the lightest structural metals available to design engineers. Mg alloys have high specific strength, are easy to machine and are potentially recyclable. These attributes make them particularly attractive for applications in the transportation industry [1,2]. However, current Mg alloys do not possess the required creep resistance above 125 °C [1]. Creep deformation in Mg alloys has been generally contributed to grain boundary sliding and plastic deformation leading to intergranular failure [**Error! Bookmark not defined.**].

Available literature suggests that zinc (Zn) and aluminum (Al) have been effectively used to increase the room temperature mechanical properties of Mg-based wrought alloys via solid-solution strengthening and dispersion strengthening with intermetallic compounds. Zn has been observed to raise the eutectic temperature thus slightly enhancing the creep resistance of some Mg alloy systems. Zn addition, however, also increased alloy's susceptibility to microporosity and embrittlement. [**Error! Bookmark not defined.**].

Mechanical properties of Al-containing Mg alloys have been extensively studied, due to their commercial relevance. The rapid loss of strength of Al-containing alloys above 120°C has been generally attributed to the presence of β-$Mg_{17}Al_{12}$ phase (with incipient melting temperature of ~430°C) at the grain triple-points. To retard formation of the β phase, addition of rare earths (REs) to Mg-Al systems was implemented. Rare earths were seen to bind aluminum and form Al_xRE_y thermally stable intermetallics. The role of cerium, lanthanum, neodymium and praseodymium on improving creep resistance, however, remains the subject of extensive research.

In the case of RE addition to wrought Mg-Zn alloy systems, the rare earths generally reduced the tendency for microporosity and embrittlement. In these alloy systems, REs have combined to form additional Al-Zn-RE intermetallics. These compounds effectively pinned the grain boundaries above 120°C and the maximum effect from RE addition was seen in the 2-6 wt% level [3,4].

One of the most advanced Al-RE-Mg alloy systems is the AE42, with 4wt% Al and 2wt%RE. Research has shown that at 150°C, the creep resistance of the AE42 alloy begins to significantly deteriorate, because lamellar $Al_{11}RE_3$ intermetallic typically located in the vicinity of the grain boundaries, begins to dissolve and the Al_2RE and β-$Mg_{17}Al_{12}$ phases appear. The $Mg_{17}Al_{12}$ phase with its low incipient melting temperature subsequently facilitates creep-induced grain boundary movement [3].

Research focusing on EZ33 alloy, with 3wt%Re and 3wt%Zn, suggests that formation of intermetallics (and their stoichiometry) in this system is complex and strongly depends on the constitutive elements of the Rare Earth mischmetal (mostly forming T-Mg_9(Ce,La,Pr,Nd) phase. In this alloy, T-phase is stable at temperatures as high as 420°C [5]. Thus, available literature suggests that at 150°C, the EZ33 alloy should have a higher creep resistance than AE42.

Experimental Setup

The alloy samples used in this research were produced by Timminco Corporation, Canada. The alloy compositions can be found in Table I. The alloys were cast using a proprietary controlled-cooling static casting process, followed by hot extrusion. Both alloys were cast and formed without cracking or other processing defects. Figure 1 shows a schematic of the torus-like extruded specimens produced for this research. The outer diameter of the torus was 25mm, inner diameter was 7mm and thickness 9mm. The torus was sectioned to reveal the cross section (i.e., surface parallel with the extrusion direction) and the radial section (i.e., surface perpendicular to the extrusion direction).

Table I. Alloy Composition

Constituents (wt%)	Alloy	
	AE42	EZ33
Al	3.5-4.5	≤0.05
Zn	≤0.20	2.0-3.1
Mn	0.20-0.50	0.20-0.50
Fe	≤0.01	≤0.01
Ni	≤0.005	≤0.005
Cu	≤0.05	≤0.05
Si	≤0.05	≤0.05
RE	1.2-3.0	2.5-3.5
Zr	0.45-0.70	

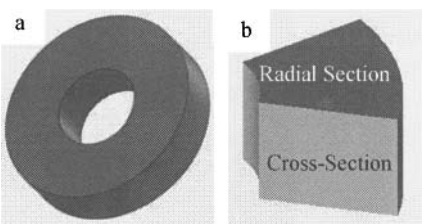

Figure 1. Alloy samples a) Extruded torus and b) Sample surfaces examined.

Nano-indentation Creep Tests

Nano-indentation tests were carried using a sapphire Berkovich indenter. Creep indentation measurements were conducted at 25°C and 150°C (±1°C) on both alloys and both sample surfaces (i.e., cross-section and radial section). For each alloy, six independent 1-hour constant load tests were performed to validate the repeatability of results. From these tests a plot of indentation depth versus time was generated and used for comparison of creep resistances of the samples.

Six indentation tests to a depth of 10 μm were performed for all samples. Based on these experiments, the applied force, F, was plotted as a function of the total indentation depth, thus enabling calculation of the elastic (h_e) and plastic (h_p) deformation of the materials. These tests were also used to calculate sample hardness, H, using Equation 1. The indenter was assumed to be a perfect pyramid and no material pile-up or sink-in occurred during indentation testing.

(Equation 1)

Creep-induced Residual Strain Measurement

High-temperature compressive creep residual strain measurements were performed at the Canadian Neutron Beam Centre in Chalk River, Canada. Detailed description of these experiments is available in earlier papers [6,7]. Creep-induced residual strain was calculated using the peak-shift method (Equation 2), where the lattice spacing of a sample, d, was obtained from Bragg's Law (Equation 3), with the wavelength of the neutron beam, λ, at 0.237nm, first order diffraction (n=1) and scattering angle, θ, measured with a wire angle detector.

(Equation 2)

$$n*\lambda = 2*d*\sin(\theta) \quad \text{(Equation 3)}$$

Creep-induced residual strain measurements for crystallographic plane were made in a direction parallel to the extrusion direction (i.e., principal strain direction). The applied load during the neutron diffraction creep tests was 50MPa at a test temperature of 150 °C for 120 hours.

Microscopic Evaluation

Metallographic samples were prepared using standard techniques for Mg alloys. Zeiss AxioObserver A1m microscope with differential interference contrast (DIC) capability enabled imaging of the grain structure of the as-extruded specimens without the need for chemical etching. Scanning electron microscopy was conducted using JEOL-6410 SEM with XEDS capability.

Results and Discussion

Neutron Diffraction Results

The solidus temperatures, T_s, for the AE42 and EZ33 alloys are 590°C and 545°C, respectively [8,9]. Thus, in relation to the alloy's solidus, the test temperatures corresponded only to $0.27T_s$ and $0.25T_s$, respectively. However, as Figure 2 illustrates, ND measurements revealed that the residual creep-induced strain in the AE42 alloy was significantly greater than that of EZ33. AE42 exhibited primary creep deformation up to ~3% (27 hrs), with steady-state creep deformation thereafter, reaching 6% at the end of the test. In contrast, EZ33 exhibited primary creep up to 0.05% (7 hrs) and subsequently steady-state creep of ~0.06% remained for the remainder of the test.

It is worth noting, that the ND method of evaluating creep resistance of the alloy provides strain data on the bulk deformation of the specimen. Thus, the contributions of the solid-solution matrix and the intermetallics located on the grain boundaries are considered together. This is particularly relevant for comparison with the following nano-indentation results.

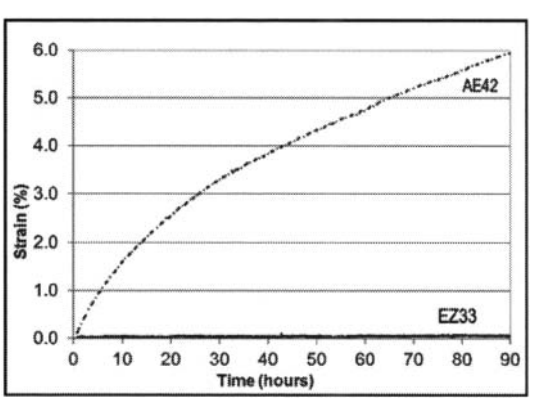

Figure 2. Compression-induced creep strain for (10 0) planes.

Nano-Indentation Results

The results of nano-indentation creep experiments are plotted in Figure 3 and Figure 4. The results confirm the same behavior as observed with ND experiments: EZ33 alloy has a higher creep resistance than AE42. However, the nano-indentation data also demonstrate that the extruded material was anisotropic, since the strain in the cross-section and radial directions varied significantly. This is in agreement with an earlier study which revealed strong tendency for the basal planes to align with the extrusion axis [10]. The pole figure (Figure 5), obtained from ND texture experiments with the AE42 and EZ33 alloy demonstrate this fact. At 150°C, Figure 3**Error! Reference source not found.**b shows that AE42 alloy began to exhibit anisotropic response, since the radial and cross-section strains continuously diverged. In the case of EZ33, the creep indentation strains remained comparable for the duration of the test.

The nano-indentation results in Figure 4 also suggest that the strain in the extrusion direction was significantly more sensitive to increase in temperature than the strain in the radial direction. This was attributed to the significantly different microstructures for these samples. As will be discussed in the following sections, the extrusion process generated high-aspect ratio grains in the extrusion direction, with non-uniform dispersion of intermetallic compounds, while the radial direction had spheroidal grains and uniformly dispersed intermetallics.

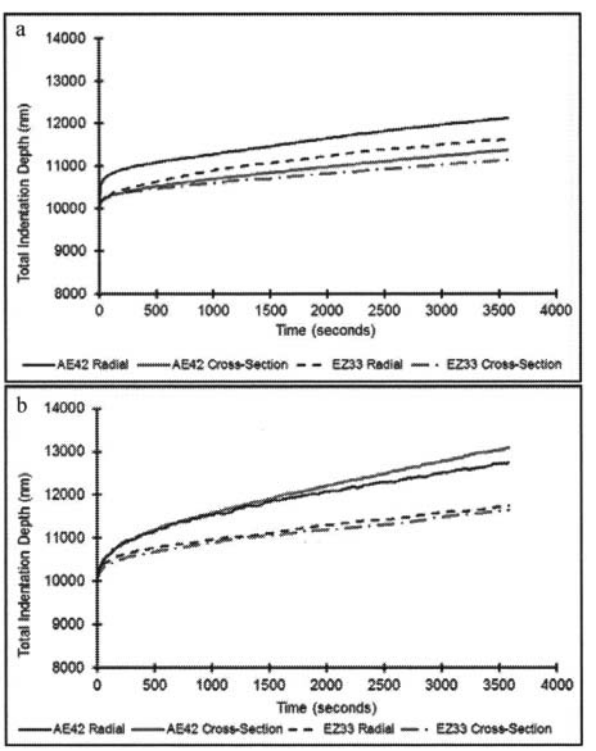

Figure 3. Nano-indentation compressive creep measurements in the radial and cross sections at a) 25°C and b) 150°C.

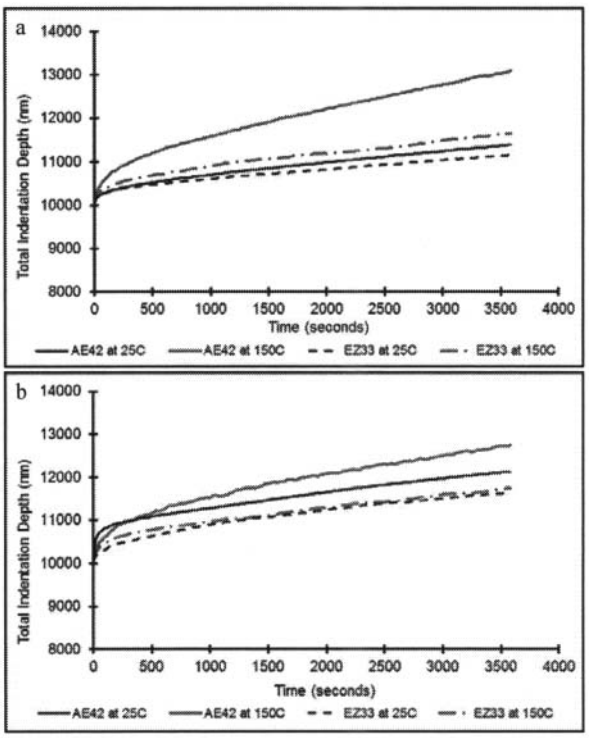

Figure 4. Nano-indentation compressive creep measurements at 25°C and 150° of the a) cross-section and b) radial section.

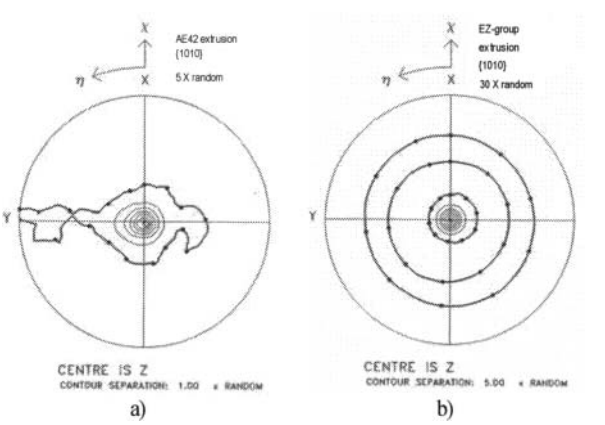

Figure 5. Pole figure for {1010} planes: a) AE42 alloy, b) EZ33 alloy.

Hardness and Elastic Modulus

The nano-indentation hardness data (Table I) directly support the creep results. On average, the EZ33 alloy was ~35% harder than the AE42 alloy. Increasing the test temperature from 25°C to 150°C resulted in ~35% and ~20% loss of strength for the EZ33 and AE42 alloys, respectively. For both alloys, the cross-section (i.e., plane parallel to extrusion direction) exhibited higher hardness than the radial plane. This is possibly the result of the presence of coherent intermetallic compounds which form on the

basal planes of the Mg matrix. Consequently, the hardness values were higher suggesting that dislocation glide along the basal planes was more difficult.

The elastic modulus data reveal that on average AE42 had 30-43% lower modulus than EZ33. The results in Table II also confirm that AE42 was significantly more anisotropic and temperature sensitive. This is possibly indicative of dislocation glide being a factor in creep deformation of this alloy.

Table I. Alloy Hardness

Alloy		Hardness (MPa)	
		25 °C test temperature	150 °C test temperature
AE42	Cross section	571 ± 30	437 ± 41
	Radial section	334 ± 16	302 ± 25
EZ33	Cross section	781 ± 50	563 ± 40
	Radial section	682 ± 83	503 ± 39

Table II. Alloy Elastic Modulus

Alloy		Elastic modulus (GPa)	
		25 °C test temperature	150 °C test temperature
AE42	Cross section	28 ± 4	33 ± 3
	Radial section	14 ± 1	19 ± 2
EZ33	Cross section	40 ± 2	40 ± 7
	Radial section	38 ± 4	39 ± 10

Alloy Microstructure

As can be seen in Figure 6, the microstructure of the alloys was highly anisotropic for the cross-section and radial directions. The hot extrusion process caused deformation of the grain boundary regions resulting in banding of intermetallics along the extrusion direction (vertical in Figure 6a), as expected. The same microstructural characteristics were observed for EZ33 alloy.

Light optical microscopy with DIC prism revealed a fundamental difference between the AE42 and EZ33 alloys in terms of the distribution of the intermetallic phases. As Figure 7 shows, the AE42 alloy contained intermetallics (predominantly acicular $Al_{11}RE_3$ and globular Al_2RE) dispersed throughout the grain boundaries as well as the matrix. In contrast, EZ33 contained intermetallics (globular $Mg_xZn_yRE_z$) exclusively on the grain boundaries. Thus, the intermetallics in the EZ33 were significantly more effective in pining the grains during high temperature deformation. Further, as Figure 8 suggests, the cuboid intermetallics in the AE42 alloy had relatively flat interface with the matrix, while in the EZ33 alloy the intermetallics were finer and with serrated edges, thereby more effectively anchoring neighboring grains.

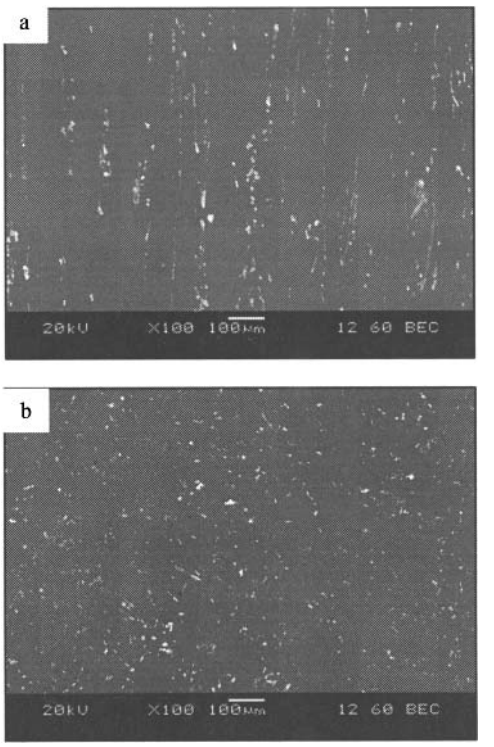

Figure 6. Microstructure of AE42 alloy (SEM image) a) Cross-section and b) Radial section.

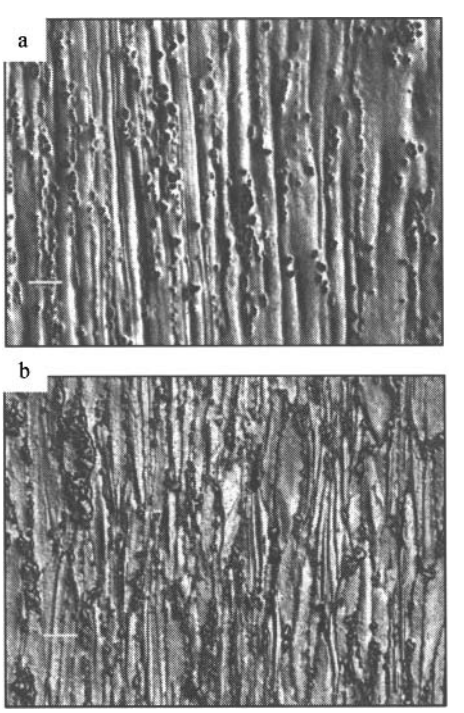

Figure 7. Microstructures for cross section surfaces. 100x; scale = 50µm (DIC polarization) a) AE42 and b) EZ33

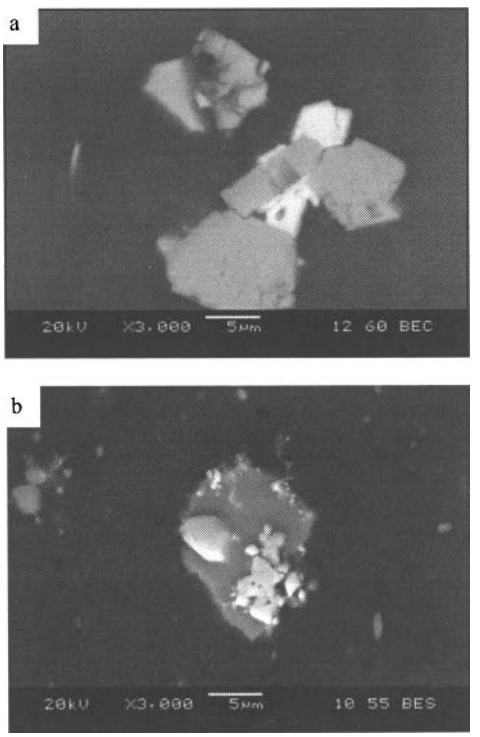

Figure 8. Morphology of intermetallics (SEM image) of a) AE42 and b) EZ33

Conclusions

This research demonstrated that neutron diffraction creep-induced residual strain measurements and nano-indentation creep measurements can be used to provide valuable data on creep performance of metallic alloys. The results of this research provided for the following conclusions:

1. AE42 was seen to be highly isotropic with properties highly sensitive to temperature variation.
2. On average, the EZ33 alloy was ~35% harder and had a 30-43% higher elastic modulus than the AE42 alloy.
3. Residual creep-induced strain in the AE42 alloy was significantly greater than that of EZ33.
4. The microstructure of the alloys was highly anisotropic for the cross-section and radial directions. Banding of intermetallics along the extrusion direction was observed in both alloys.
5. AE42 alloy contained acicular and globular intermetallics dispersed throughout the grain boundaries as well as the matrix.
6. EZ33 contained fine and irregular intermetallics exclusively on the grain boundaries, which significantly enhanced the creep-resistance of the alloy.

Acknowledgement

The authors would like to acknowledge the financial support of the Natural Sciences and Engineering Research Council of Canada for financial support and Mr. S. Shook for material donation.

References

1. M. Avedesian and H. Baker, *ASM Specialty Handbook; Magnesium and Magnesium Alloys,* (Materials Park: ASM International, 1999), 3-239.

2. E. Emley, *Principles of Magnesium technology* (New York: Pergamon Press, 1966), 42.

3. B. R. Powell et al., "Microstructure and Creep Behaviour in AE42 Magnesium Die-Casting Alloy," *JOM*, 54 (8) (2002), 34-38.

4. L. Peng, F. Yang, J. Nie, and J.C.M. Li, "Impression creep of a Mg-8Zn-4Al-0.5Ca alloy," *Materials Science and Engineering A,* 410-411 (2005), 42-47.

5. T. Rypaev et al., "Microstructure of superplastic QE22 and EZ33 magnesium alloys," *Materials Letters*, 62 (2008), 4041-4043.

6. D. Sediako and M. Gharghouri, "Neutron Diffraction Measurements of Residual Stress in Creep Resistant Mg Alloys," *Magnesium Technology 2008*, TMS, 2008, 407-409.

7. D. Sediako and S. Shook, "Application of Neutron Diffraction in In-Situ Studies of Stress Evolution in High Temperature Creep Testing of Creep-resistant Mg Alloys," *Magnesium Technology 2009*, TMS, 2009, 255-259.

8. K. Mills, *Recommended Values of Thermophysical Properties for Selected Commercial Alloys,* (Cambridge, England: ASM International, 2002), 143-157.

9. International Magnesium Association. *Melting point/range for Magnesium.* Accessed: September 14, 2010: http://www.intlmag.org/phys07.html

10. S. Shook, and D. Sediako, "Analysis Of Stress Evolution in High Temperature Creep Testing of Creep-resistant Mg Alloys," *IMI – 2009*, San Francisco, 43-51.